Broadly tunable dual-wavelength light source for coherent anti-Stokes Raman scattering microscopy

Feruz Ganikhanov, Silvia Carrasco, and X. Sunney Xie

Department of Chemistry and Chemical Biology, Harvard University, 12 Oxford Street, Cambridge, Massachusetts 02138

Mordechai Katz

Electro-Optics Division, Soreq NRC, Yavne 81800, Israel

Wolfgang Seitz and Daniel Kopf

High-Q-Laser Production GmbH, Kaiser-Franz-Josef-Strasse 61, A-6845 Hohenems, Austria

Received January 13, 2006; revised February 8, 2006; accepted February 10, 2006; posted February 14, 2006 (Doc. ID 67256)

The signal and idler beams from a picosecond, synchronously pumped optical parametric oscillator (OPO) provide the two colors necessary for coherent anti-Stokes Raman scattering (CARS) microscopy. The OPO provides a continuously tunable frequency difference between the two beams over a broad range of Raman shifts ($100-3700\,\mathrm{cm}^{-1}$) by varying the temperature of a single nonlinear crystal. The near-infrared output (900–1300 nm) allows for deep penetration into thick samples and reduced nonlinear photodamage. Applications of this light source to *in vivo* cell and *ex vivo* tissue imaging are demonstrated. © 2006 Optical Society of America

OCIS codes: 190.4410, 110.0180.

Nonlinear optical phenomena have been used as powerful imaging techniques with applications in biology and medicine.[1,2] Coherent anti-Stokes Raman scattering (CARS) microscopy[2] is a high-sensitivity nonlinear technique that is noninvasive and has chemical selectivity. In the CARS process light is coherently scattered from Raman active vibrational resonances of a sample, resulting in a strong signal that allows for label-free, high-speed imaging. To generate CARS at least two optical fields with frequencies ω_p and ω_s, called pump and Stokes fields, respectively, are required. When the frequency difference $\omega_p-\omega_s$ is tuned to the frequency of a Raman-active molecular vibration (Ω), the resonantly enhanced anti-Stokes signal is generated at frequency $\omega_{as}=2\omega_p-\omega_s$.

Developments in laser sources have been essential for the advances in CARS microscopy.[2] Laser sources have evolved from low-repetition-rate femtosecond amplified systems,[3] to electronically synchronized high-repetition-rate picosecond sources,[4] to the current state-of-the-art synchronously pumped OPO systems.[5] Broadband laser systems for CARS spectroscopy, though less successful in imaging, have also been used.[6] An ideal CARS microscopy source would be a compact, turnkey laser system that has broad tunability and optimizes the spatial resolution, penetration depth, and nonlinear photodamage.

In this Letter we demonstrate a simple laser source for CARS microscopy that meets the above requirements. In particular, a broadly tunable picosecond OPO based on a periodically poled $KTiOPO_4$ (PPKTP) crystal is synchronously pumped by the second-harmonic (532 nm) output of a mode-locked $Nd:YVO_4$ laser. The OPO is continuously tunable from degeneracy (1064 nm) to 890 nm for its signal beam and to 1325 nm for its idler beam. By using the signal and idler beams as the pump and Stokes beams for CARS, respectively, it is possible to cover the entire chemically important vibrational frequency range of $100-3700\,\mathrm{cm}^{-1}$. With this new laser system we demonstrate CARS imaging in biological systems. We also show higher tissue penetration depth than previously possible by making use of the longer-wavelength output of this OPO.

The experimental setup is shown in Fig. 1. Six picosecond-long pulses at 532 nm with a 80 MHz repetition rate were delivered by a frequency-doubled, passively mode-locked $Nd:YVO_4$ laser (Hi-Q Laser production, Austria). The maximum available average power of the laser was 5 W. The OPO gain

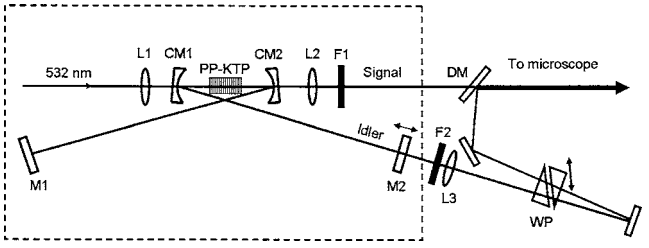

Fig. 1. OPO resonator and external layout used for CARS microscopy. The OPO is singly resonant within the idler beam wavelength range. CM1, CM2, OPO cavity concave ($r=100$ mm) mirrors with high reflection ($R>99\%$) in the idler beam wavelength range. CM2 has 70%–80% transmission at the signal beam wavelengths. M1, high-reflecting mirror; M2, 10% output coupler for the idler beam; F1, F2, long-pass filters, >850 nm; L1, L2, L3, lenses with focal lengths of 50, 150, and 1000 mm, respectively; DM, dichroic mirror; WP, wedged plates for delay control.

0146-9592/06/091292-3/$15.00

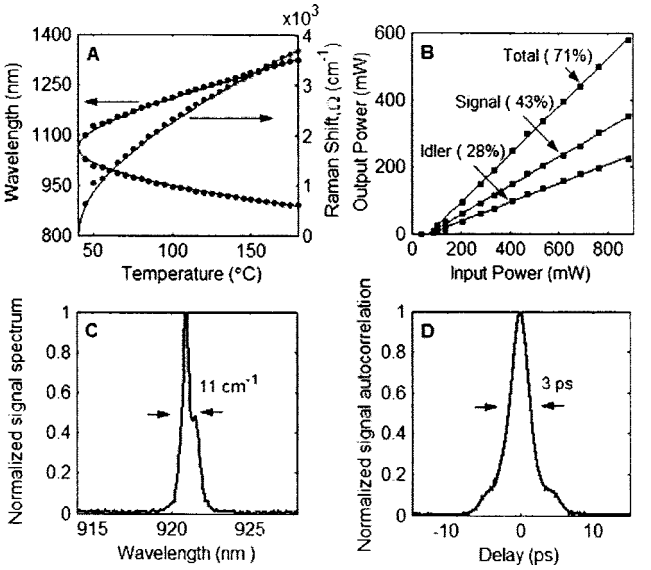

Fig. 2. A, Experimental (filled circles) wavelength tuning curve and accessible Raman frequencies as a function of the crystal temperature. The solid curves are result of the calculations. B, OPO output power versus pump power at the crystal facet. C and D show the typical signal pulse spectrum and autocorrelation trace at the OPO cavity detuning of minus 36 μm, respectively.

material is a 10.8–mm-long flux-grown KTP crystal, Z cut and poled with a grating period of $\Lambda = 8.99$ μm, satisfying first-order phase matching for second-harmonic generation at $\sim 41°$C.[7] The PP-KTP crystal was antireflection coated at a target wavelength of 1064 nm. The OPO details are shown in Fig. 1. The distances between the pump focusing lens, concave mirrors, and the crystal were close to the calculated values obtained assuming optimal focusing conditions for parametric waves.[8] With this cavity design extremely low pumping thresholds of ~ 40 mW have been achieved at 924/1254 nm signal/idler wavelength combination.

The theoretical tuning curve based on the KTP material's refractive index data,[7] the measured values, and the corresponding Raman shifts as a function of temperature are shown in Fig. 2A. At the maximum set crystal temperature of 180°C the corresponding OPO signal (pump) and idler (Stokes) pair of wavelengths are 889.4 nm and 1323.9 nm, respectively, corresponding to a Raman shift of 3690 cm^{-1}.

The signal, idler, and total powers are plotted versus the input pump power in Fig. 2B when the OPO crystal is maintained at temperature 132°C to deliver signal and idler beams at wavelengths of 921 nm and 1260 nm, respectively. We observe linear slope efficiencies for the signal and idler of 43% and 28%, respectively. Output powers for both beams were fairly constant with an $\sim 10\%-15\%$ margin throughout the tuning range at fixed pump power.

At maximum output power the OPO delivers pulses with a typical power spectrum of ~ 100 cm^{-1} (FWHM) and pulse widths of ~ 7.5 ps. When in the appropriate regime of group-velocity mismatch and at certain parametric gain values, a variety of intensity profiles and spectra can be observed.[9] In our case, for example, at an input pump power of 715 mW and under a negative single-pass cavity detuning of 36 μm, spectral narrowing down to ~ 11 cm^{-1} (Fig. 2C) occurs, leading to a less chirped pulse (~ 1.6 times transform limited, when a Gaussian pulse is assumed). The spectral bandwidth and rather small amount of chirp is still in a favorable range[10] to achieve high-contrast resonant CARS imaging. The negative detuning resulted in a 20% power drop from the maximum level. Therefore nearly optimal performance for CARS imaging and reliable long-term day-to-day operation at various crystal temperatures was possible without any passive spectral filtering element in the cavity. The OPO delivered signal and idler beams with nearly TEM_{00} far-field spatial profiles throughout the tuning range.

The signal and idler beams were outcoupled from the cavity according to the optical layout shown in Fig. 1. The idler pulse was delayed and spatially combined with the signal on a dichroic mirror. The two beams were coupled into a scanning microscope (Olympus, FV300/IX70) with a 1.2 numerical-aperture water-immersion objective lens (60×, IR UPlanApo, Olympus). Long-pass filters were used to block the OPO outputs at shorter wavelengths. The two lenses in the output beam paths were used to achieve optimal spot sizes at the objective lens entrance pupil. The total average power in the image plane of the microscope was less than 30 mW.

To determine the spatial resolution of the system, we imaged various sized polystyrene beads at a Raman shift of 2850 cm^{-1} achieved by choosing a signal–idler pair at wavelengths of 924 and 1254 nm. The characteristic lateral (xy) and longitudinal (z) resolutions were diffraction limited to approximately 420 nm and ~ 1.1 μm (FWHM), respectively.

To demonstrate the versatility and robustness of the laser source, we present a series of CARS images for different Raman shifts. Figure 3A shows an image of polystyrene beads at the C=C stretching frequency of ~ 1600 cm^{-1}. Figure 3B shows the image of a living mouse fibroblast cell (NIH-3T3-L1) cultured with deuterium-labeled oleic acid imaged at the CD_2 symmetric stretch (2100 cm^{-1}). The strong signals arise from high-density lipid droplets. The same cell type cultured in deuterium-free media is shown in Fig. 3C with the Raman shift tuned to the 2850 cm^{-1} symmetric CH_2 stretching frequency. To image with the OH stretching vibration at 3375 cm^{-1}, we prepared POPS [(l-palmitoyl-2-oleoyl-*sn*-glycero-3-phospho-L-serine)] vesicles of lipids and water.[11] The corresponding image of the 5 μm sized structure containing water is shown in Fig. 3D.

Our CARS source is optimized to image highly heterogeneous tissue samples. It is well known that the Rayleigh scattering cross section for a media with subwavelength-size features is inversely proportional to the fourth power of the wavelength. Therefore longer pump and Stokes wavelengths should increase the depth of penetration into tissue. With our system operating in the 900–1300 nm range, water absorption due to direct IR transitions is negligible.

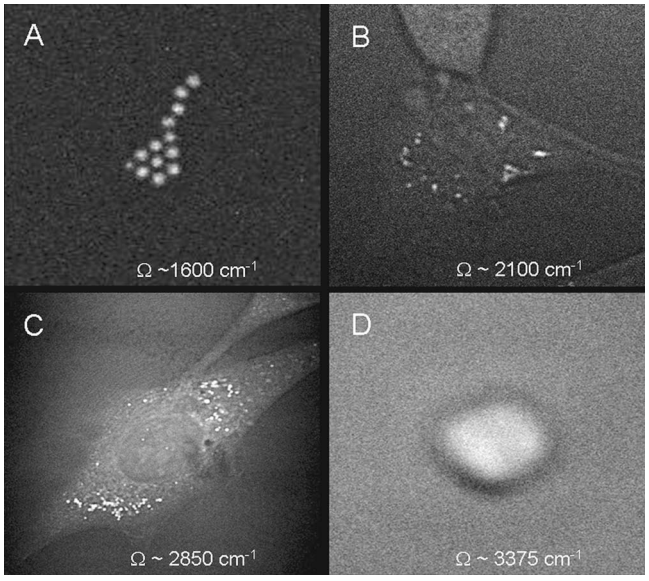

Fig. 3. CARS images at different Raman shifts. A, 1.5 μm diameter polystyrene beads imaged at the C=C stretching vibrational frequency, 1600 cm^{-1}. B, NIH 3T3-L1 cell cultured with deuterium-labeled oleic acid imaged at the CD_2 symmetric stretching vibration, 2100 cm^{-1}. Image size, 47 μm $\times$ 47 μm. C, NIH 3T3-L1 cell imaged at the CH_2 symmetric stretching vibration, 2850 cm^{-1}. Image size, 78 μm $\times$ 78 μm. D, 5 μm size POPS multilamellar vesicle imaged at the OH stretch, 3375 cm^{-1}.

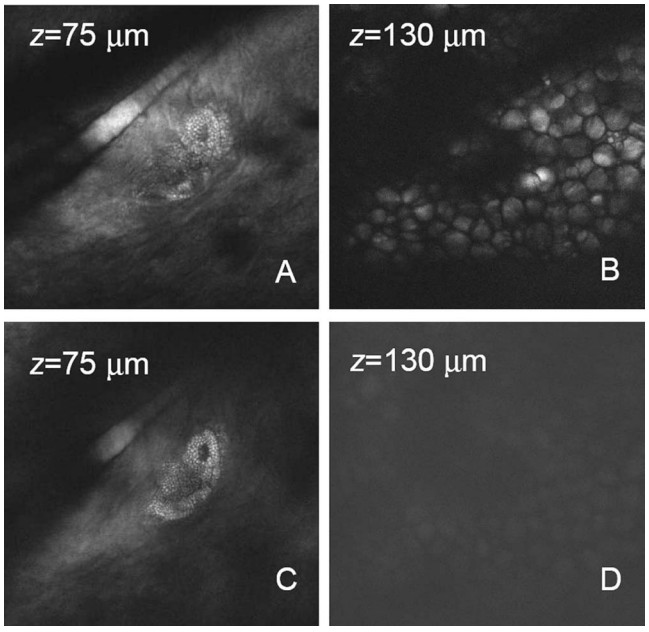

Fig. 4. Forward CARS images of mouse ear tissue at the aliphatic CH_2 stretching frequency, 2850 cm^{-1}, at two different depths of $z = 75$ μm and $z = 130$ μm, taken with two different sources. A, B, the OPO. C, D, the two picosecond-Ti:sapphire-lasers-based system.

To prove this point, we compared the CARS imaging penetration depth of this OPO to that of a synchronized Ti:sapphire[4] system. An example is shown in Fig. 4. Here, lipid-rich structures of a mouse ear at different penetration depths from the skin surface were imaged by tuning into the CH stretching vibrational band, using the new OPO (upper row, $\lambda_{pump} = 924$ nm; $\lambda_{stokes} = 1254$ nm) and the two synchronized Ti:sapphire lasers[4] (bottom row, $\lambda_{pump} = 710$ nm; $\lambda_{stokes} = 890$ nm). For intermediate penetration depths (Figs. 4A and 4C) no significant differences are observed between the two systems. However, for large penetration depths, as is the case of 130 μm in Figs. 4B and 4D, the resonant lipid-rich adipocytes are clearly visible only with the OPO system. The longer wavelength OPO allowed for penetration depths almost 70 μm deeper than the Ti:sapphire system.

Multiphoton processes caused by the high peak power of ultrafast pulses significantly contribute to sample photodamage[12]; these processes are reduced at longer excitation wavelengths. No cell photodamage that would result in changed morphology was observed at our excitation powers for the wavelengths provided by this OPO. In the experiments with living cells we had maximum exposure time of 10 min to the above quoted power.

In conclusion, we have demonstrated a compact laser source based on a novel picosecond OPO for CARS microscopy. The stable operation, broad tunability with a single nonlinear crystal, and improved penetration depth make it an optimal source for CARS imaging in chemical and biomedical research.

We appreciate help from C. Evans, B. Saar, W. Yang, and X. Nan of Harvard University; I. Rimke and E. Buettner of APE, Berlin; D. Hum and M. M. Fejer of Stanford University. This work was supported by NIH Director's Pioneer Award to X. S. Xie. S. Carrasco thanks the Fulbright Program and the Spanish Ministry of Education and Science. X. S. Xie's e-mail address is xie@chemistry.harvard.edu.

References

1. Special issue: Optical Imaging, Nat. Biotechnol. **21**(11), (2003).
2. J.-X. Cheng and S. Xie, J. Phys. Chem. B **108**, 827 (2004).
3. M. Hashimoto, T. Araki, and S. Kawata, Opt. Lett. **25**, 1768 (2000).
4. E. O. Potma, D. J. Jones, J. X. Cheng, X. S. Xie, and J. Ye, Opt. Lett. **27**, 1168 (2002).
5. C. L. Evans, E. O. Potma, M. Puoris'haag, D. Cote, C. P. Lin, and X. S. Xie, Proc. Natl. Acad. Sci. U.S.A. **102**, 16807 (2005).
6. T. W. Kee and M. T. Cicerone, Opt. Lett. **29**, 2101 (2004).
7. S. Emanueli and A. Arie, Appl. Opt. **42**, 6661 (2003).
8. G. D. Boyd and D. A. Kleinman, J. Appl. Phys. **39**, 3597 (1970).
9. S. A. Akhmanov and K. N. Drabovich, IEEE J. Quantum Electron. **QE-4**, 598 (1968).
10. J.-X. Cheng, A. Volkmer, L. D. Book, and X. S. Xie, J. Phys. Chem. B **105**, 1277 (2001).
11. J.-X. Cheng, S. Pautot, D. A. Weitz, and X. S. Xie, Proc. Natl. Acad. Sci. U.S.A. **100**, 9826 (2001).
12. A. Hopt and E. Neher, Biophys. J. **80**, 2029 (2001).